Chapter 9: Understanding and Attributing Climate Change
Figures

Coordinating Lead Authors: Gabriele C. Hegerl (USA), Francis W. Zwiers (Canada)

Lead Authors: Pascale Braconnot (France), Nathan P. Gillett (Canada), Yong Luo (China), Jose Marengo (Brazil), Neville Nicholls (Australia), Joyce E. Penner (USA), Peter A. Stott (UK)

Contributing Authors: M. Allen (UK), C. Ammann (USA), N. Andronova (USA), R.A. Betts (UK), A. Clement (USA), W. Collins (USA), S. Crooks (UK), T. Delworth (USA), C. Forest (USA), P. Forster (UK), H. Goosse (Belgium), J. Gregory (UK), D. Harvey (Canada), G.S. Jones (UK), F. Joos (Switzerland), J. Kenyon (USA), J. Kettleborough (UK), V. Kharin (Canada), R. Knutti (Switzerland), H. Lambert (UK), M. Lavine (USA), T. Lee (Canada), D. Levinson (USA), V. Masson-Delmotte (France), T. Nozawa (Japan), B. Otto-Bliesner (USA), D. Pierce (USA), S. Power (Australia), D. Rind (USA), L. Rotstayn (Australia), B. D. Santer (USA), C. Senior (UK), D. Sexton (UK), S. Stark (UK), D. Stone (UK), S. Tett (UK), P. Thorne (UK), R. van Dorland (The Netherlands), M. Wang (USA), B. Wielicki (USA), T. Wong (USA), L. Xu (USA, China), X. Zhang (Canada), E. Zorita (Germany, Spain)

Review Editors: David Karoly (USA, Australia), Laban Ogallo (Kenya), Serge Planton (France)

Date of Draft: 27 October 2006

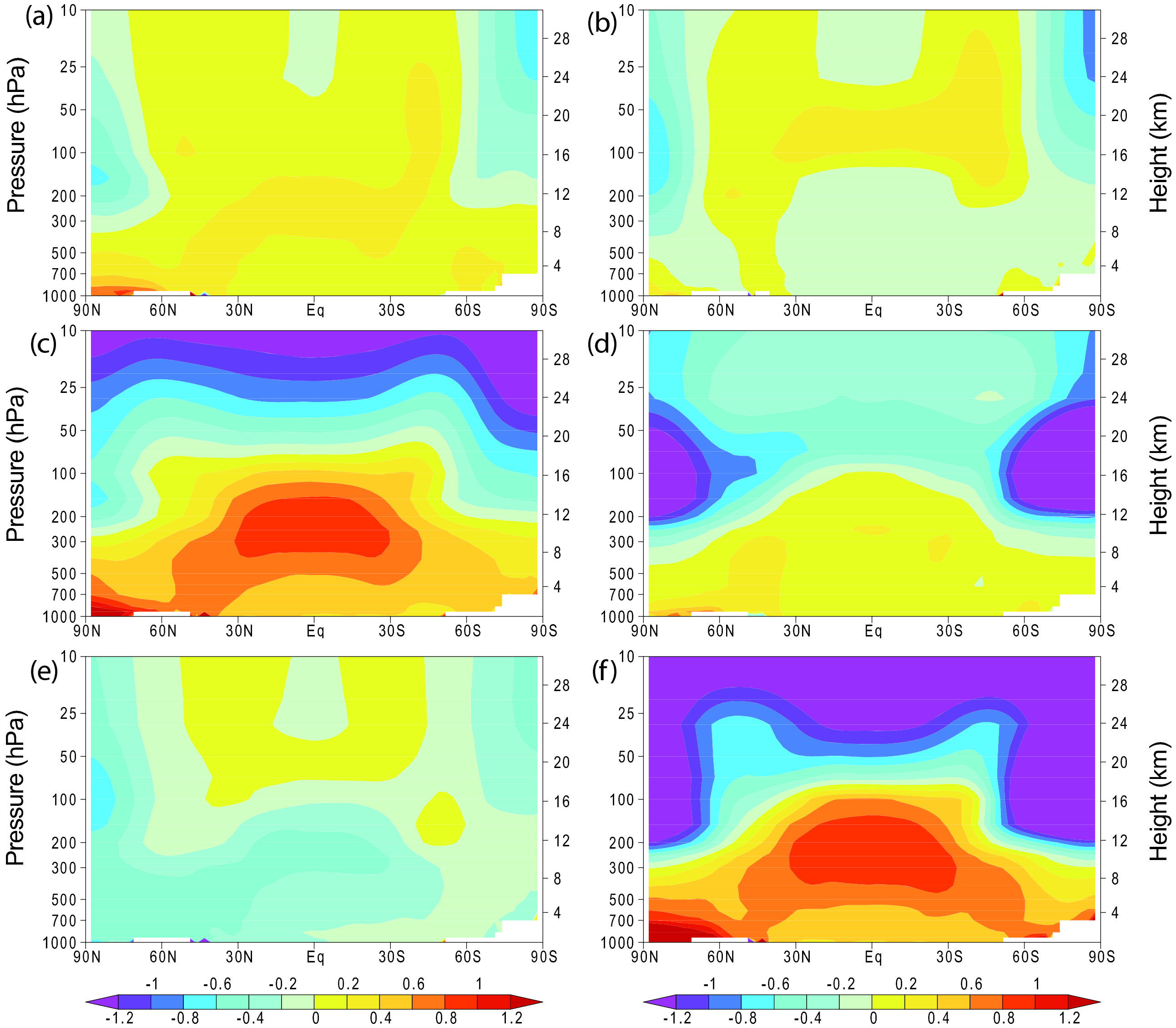

Figure 9.1. Zonal mean atmospheric temperature change from 1890 to 1999 (°C/Century) as simulated by the PCM model from (a) solar forcing, (b) volcanoes, (c) well-mixed greenhouse gases, (d) tropospheric and stratospheric ozone changes, (e) direct sulphate aerosol forcing, and (f) the sum of all forcings. Plot is from 1000 hPa to 10 hPa (shown on left scale) and from 0 km to 30 km (shown on right). See Appendix 9.C for additional information. Based on Santer et al. (2003a).

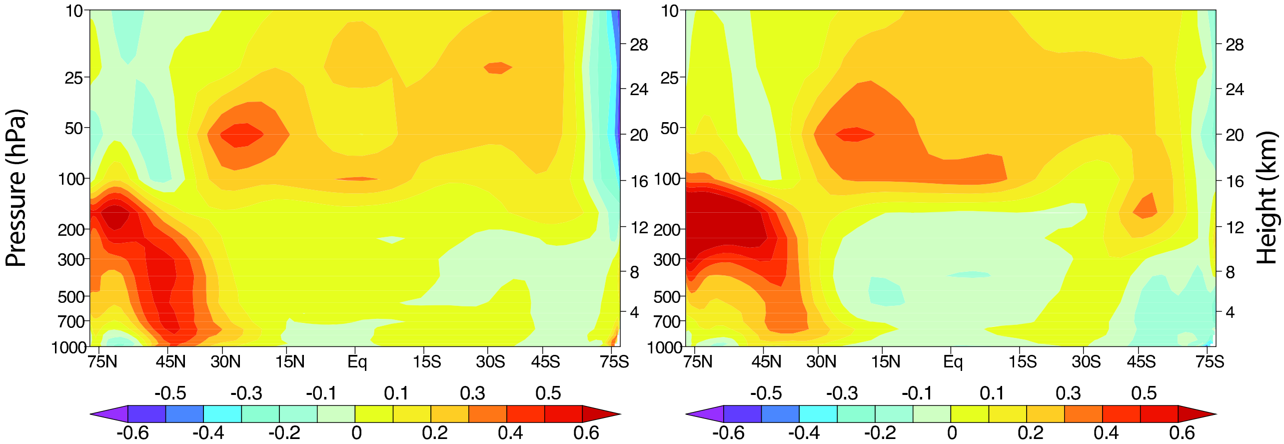

Figure 9.2. The zonal mean equilibrium temperature change (°C) between a present-day minus a preindustrial simulation of the CSIRO atmospheric model coupled to a mixed-layer ocean model from (a) direct forcing from fossil fuel black carbon and organic matter (BC+OM) and (b) the sum of fossil fuel BC+OM and biomass burning. Plot is from 1000 hPa to 10 hPa (shown on left scale) and from 0 km to 30 km (shown on right). Note the difference in colour scale from Figure 9.1. See Appendix 9.C for additional information. Based on Penner et al. (2005)

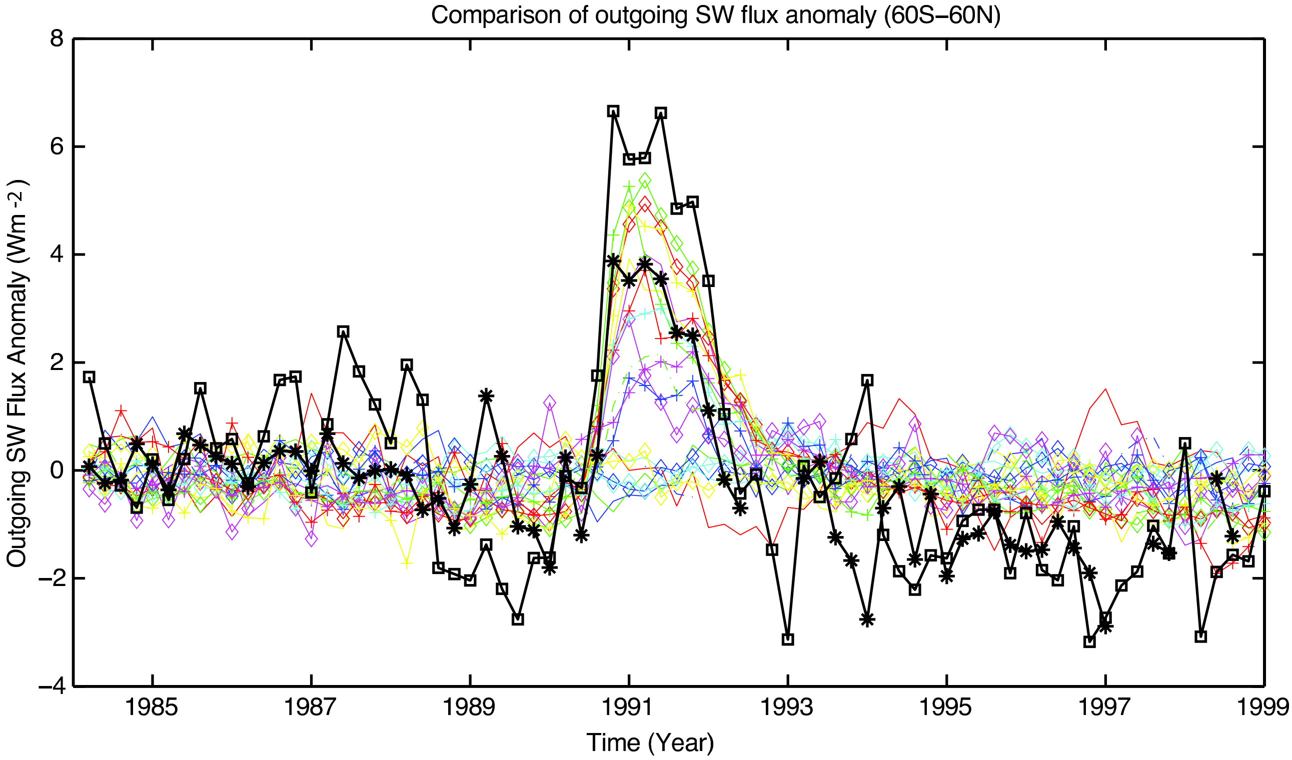

Figure 9.3. Comparison of outgoing shortwave flux anamolies (in W/m^2) (calculated relative to the entire time period) from several models in the multi-model archive at PCMDI (coloured curves) with ERBS satellite data (black with stars; Wong et al., 2006)and with the ISCCP FD data set (black with squares, Zhang et al., 2004). Models shown are CCSM3, CGCM3.1(T47), CGCM3.1(T63), CNRM-CM3, CSIRO-MK3.0, FGOALS-g1.0, GFDL-CM2.0, GFDL-CM2.1, GISS-AOM, GISS-EH, GISS-ER, INM-CM3.0, IPSL-CM4, MRI-CGCM2.3.2 (model IDs 3-7, 10-17 and 20, Chapter 8, Table 8.1). The comparison is restricted to 60ºS–60ºN because the ERBS data are considered more accurate in this region. Note that not all models included the volcanic forcing from Pinatubo (1991–1993) and so do not predict the observed increase in outgoing solar radiation. See Appendix 9.C for additional information.

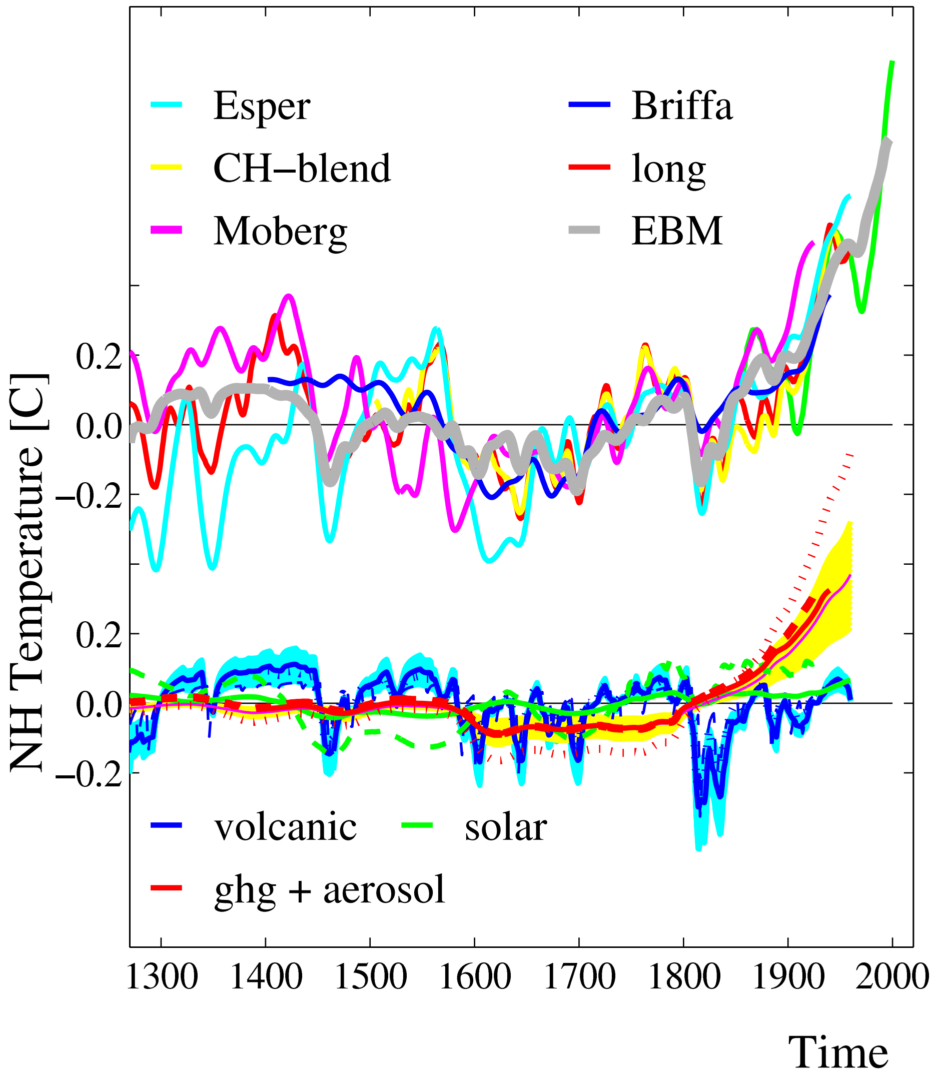

Figure 9.4. Contribution of external forcing to several high-variance reconstructions of Northern Hemispheric temperature (Esper et al. (2002), (Hegerl et al., 2006b; termed CH-blend and CH-blend long), Moberg et al. (2005), and Briffa et al. (2001)). The *top panel* compares reconstructions to an Energy Balance climate model (EBM) simulation (equilibrium climate sensitivity of 2.5ºC) of NH 30–90ºN average temperature, forced with volcanic, solar, and anthropogenic forcing. Instrumental temperature data are shown by a green line. All data are smoothed removing variance below 20 yrs. The *bottom panel* shows the estimated contribution of the response to volcanic (blue lines with blue uncertainty shade), solar (green) and greenhouse gas and aerosol forcing (red line with yellow shades, aerosol only in 20th century) to each reconstruction. The estimates are based on multiple regressions of the reconstructions on fingerprints for individual forcings. The contributions to different reconstructions are indicated by different linestyles (Briffa et al: solid, fat, Esper et al: dotted, Moberg: dashed and Ch-blend: solid, thin, with shaded 90% confidence limits around best estimates for each detectable signal). All reconstructions show a highly significant volcanic signal, and all but Moberg et al. (which ends in 1925) a detectable greenhouse gas signal at the 5% significance level. The latter shows a detectable greenhouse gas signal with less significance. Only Moberg et al. contains a detectable solar signal (only shown for these data and CH-blend, where it is not detectable). Forcing fingerprints are centered to the period analyzed, and all data are decadally averaged. The reconstructions represent slightly different regions and seasons: Esper et al. (2002) is calibrated to 30–90N land temperature, CH-blend and CH-blend (long) (Hegerl et al., 2006b) to 30–90N mean temperature, and Moberg et al. (2005) to 0–90N temperature. From (Hegerl et al., 2006b).

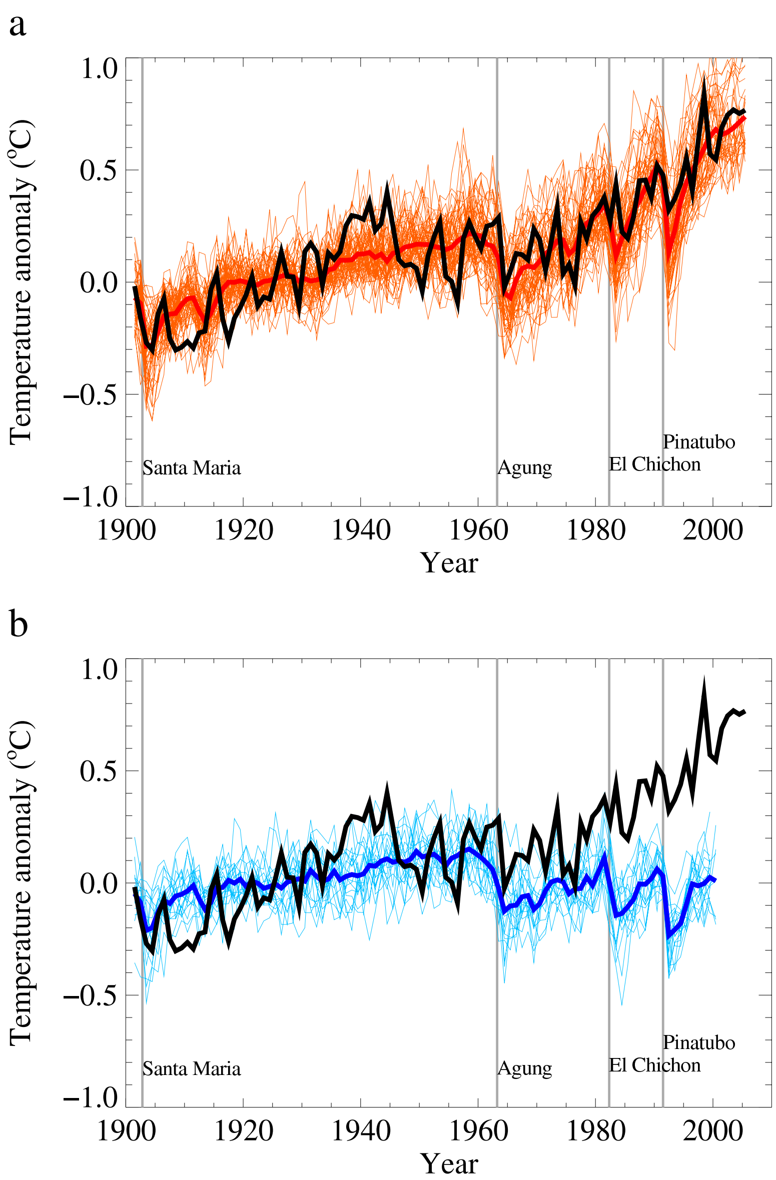

Figure 9.5. Comparison between global mean temperature anomalies from observations (black) and AOGCM simulations forced with (a) both anthropogenic and natural forcings and (b) natural forcings only. All data are shown as global mean tempeature anomalies relative to the period 1901–1950, as observed (black, HadCRUT3, Brohan et al., 2006) and, in (a) as obtained from 58 simulations produced by 14 models with both anthropogenic and natural forcings. The multimodel ensemble mean is shown as a thick red curve and individual simulations are shown as thin red curves. Vertical grey lines indicate the timing of major volcanic events. Those simulations that ended before 2005 were extended to 2005 by using the first few years of the SRES A1B scenario simulations that continued from the respective 20th century simulations, where available. The simulated global mean temperature anomalies in (b) are from 19 simulations produced by 5 models with natural forcings only. The multimodel ensemble mean is shown as a thick blue curve and individual simulations are shown as thin blue curves. Simulations are selected that do not exhibit excessive drift in their control simulations (no more than 0.2ºC per century). Each simulation was sampled so that coverage corresponds to that of the observations. Further details of the models included and the methodology for producing this figure are given in Appendix 9.C. Units: ºC. After Stott et al. (2006b).

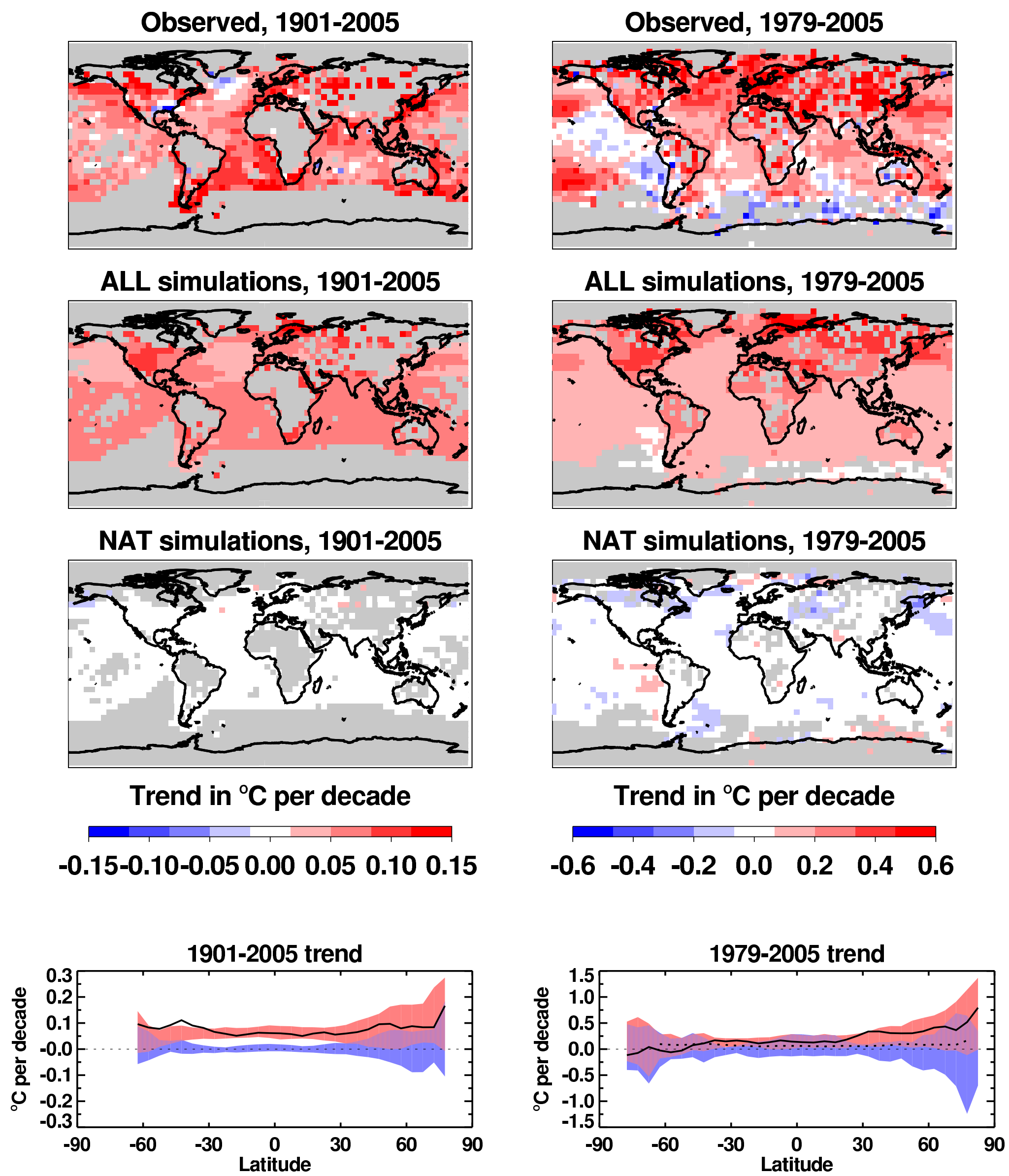

Figure 9.6. Trends in observed and simulated temperature changes over the 1901–2005 (left column) and 1979–2005 (right column) periods. *First row:* trends in observed temperature changes (HadCRUT3, Brohan et al., 2006). *Second row:* average trends in 58 historical simulations from 14 climate models including both anthropogenic and natural forcings. *Third row:* average trends in 19 historical simulations from 5 climate models including natural forcings only. Grey shading in top three rows indicates regions where there are insufficient observed data to calculate a trend for that grid box (see Appendix 9.C for further details of data exclusion criteria). *Fourth row:* average trends for each latitude; observed trends are indicated by solid black curves. Red shading indicates the middle 90% range of trend estimates from the 58 simulations including both anthropogenic and natural forcings (estimated as the range between 4th and 55th of the 58 ranked simulations); blue shading indicates the middle 90% range of trend estimates from the 19 simulations with natural forcings only (estimated as the range between 2nd and 18th of the 19 ranked simulations); for comparison, the dotted black curve in the right hand plot shows the observed 1901–2005 trend. Note that scales are different between columns. The "ALL" simulations were extended to 2005 by adding their SRES A1B continuation runs where available. Where not available, and in the case of the NAT simulations, the mean for the 1996–2005 decade was estimated using model output from 1996 to the end of the available runs. In all plots, each climate simulation was sampled so that coverage corresponds to that of the observations. Further details of the models included and the methodology for producing this figure are given in Appendix 9.C. Units: ºC.

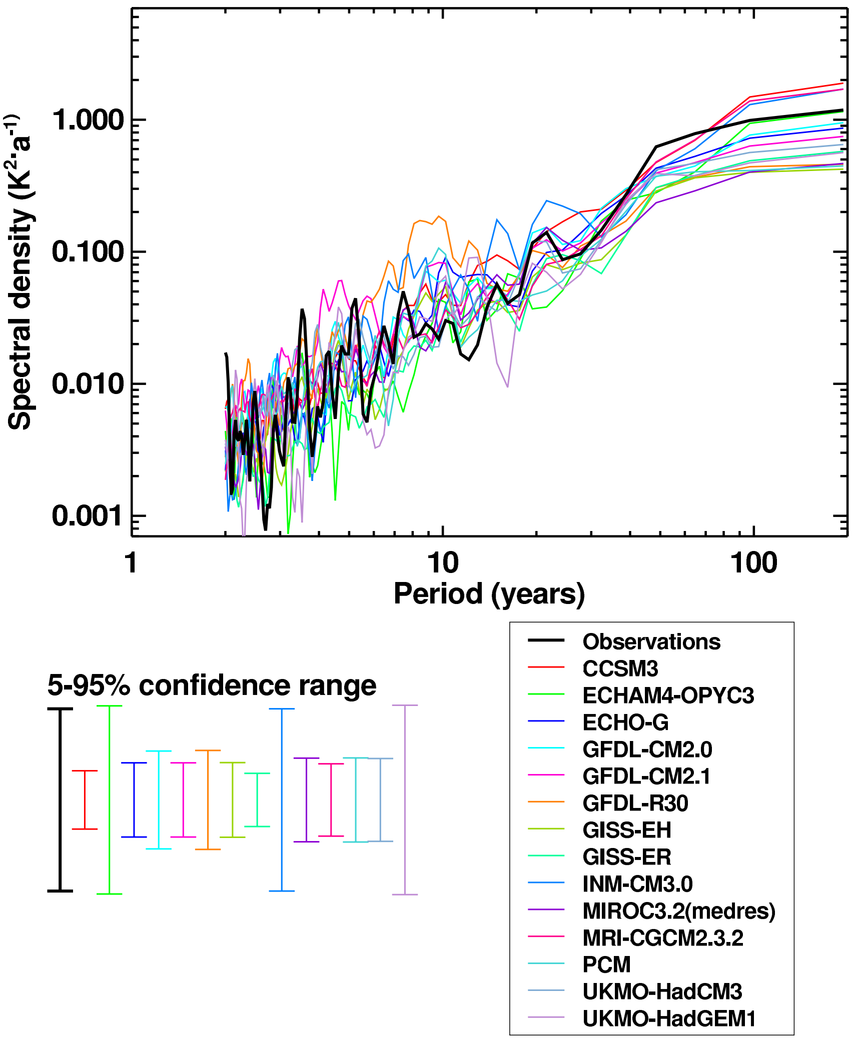

Figure 9.7. Comparison of variability as a function of time scale of annual global mean temperatures from the observed record (HadCRUT3, Brohan et al., 2006) and from AOGCM simulations including both anthropogenic and natural forcings. All power spectra are estimated using a Tukey-Hanning filter of width 97 years. The model spectra displayed are the averages of the individual spectra estimated from individual ensemble members. The same 58 simulations and 14 models are used as in Figure 9.5a. All models simulate variability on decadal timescales and longer that is consistent with observations at the 10% significance level. Further details of the method of calculating the spectra are given in Appendix 9.C. Units: $^{o}C^{2}$/year.

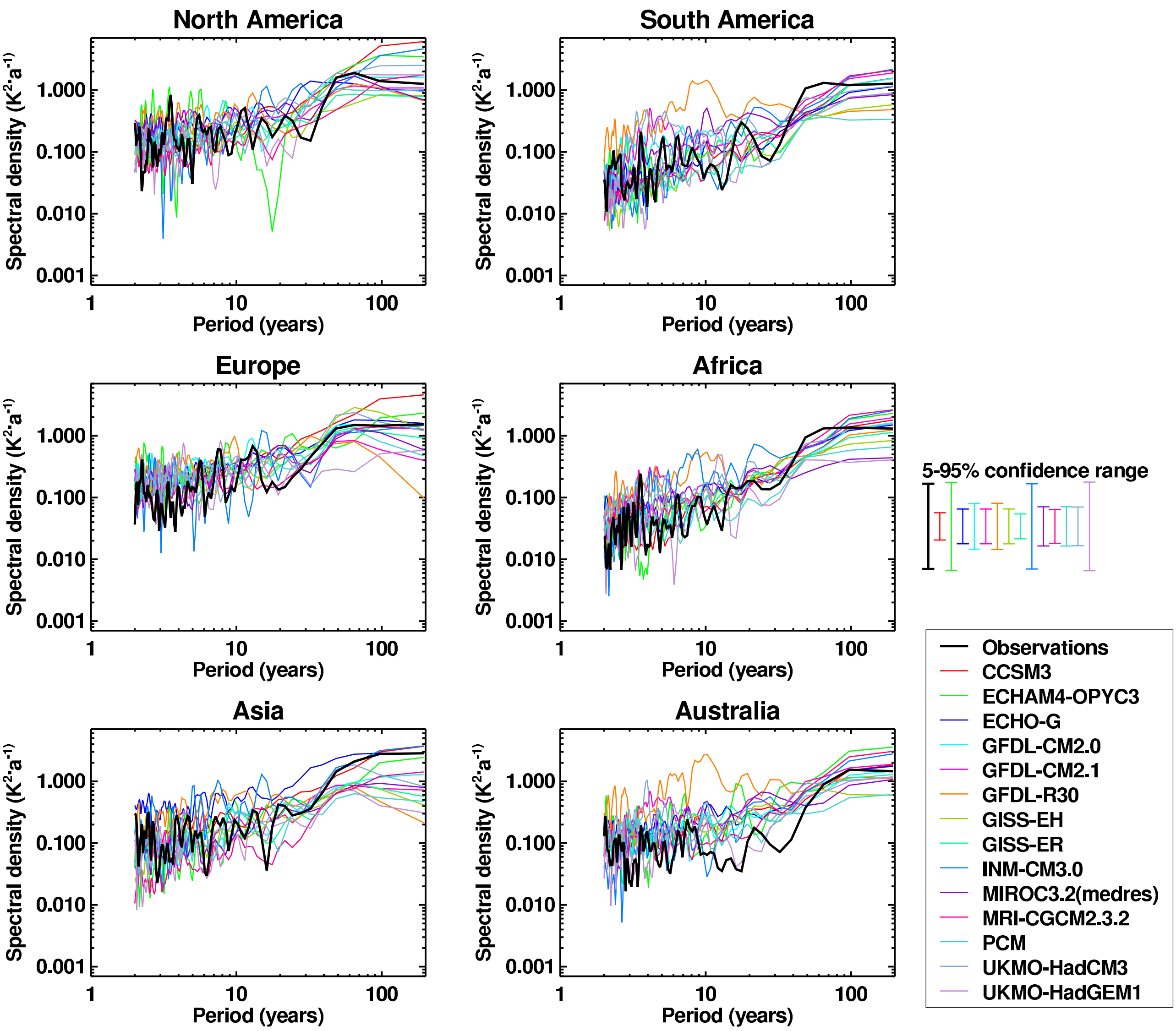

Figure 9.8. As Figure 9.7, except for continental mean temperature for continental regions defined by combining two or more sub-continental regions. Spectra calculated in the same manner as Figure 9.7. See Appendix 9.C for a description of the regions and for details of the method used. Models simulate variability on decadal timescales and longer that is consistent with observations in all cases except 2 models over South America, 5 models over Asia and and 2 models over Australia (at the 10% significance level).

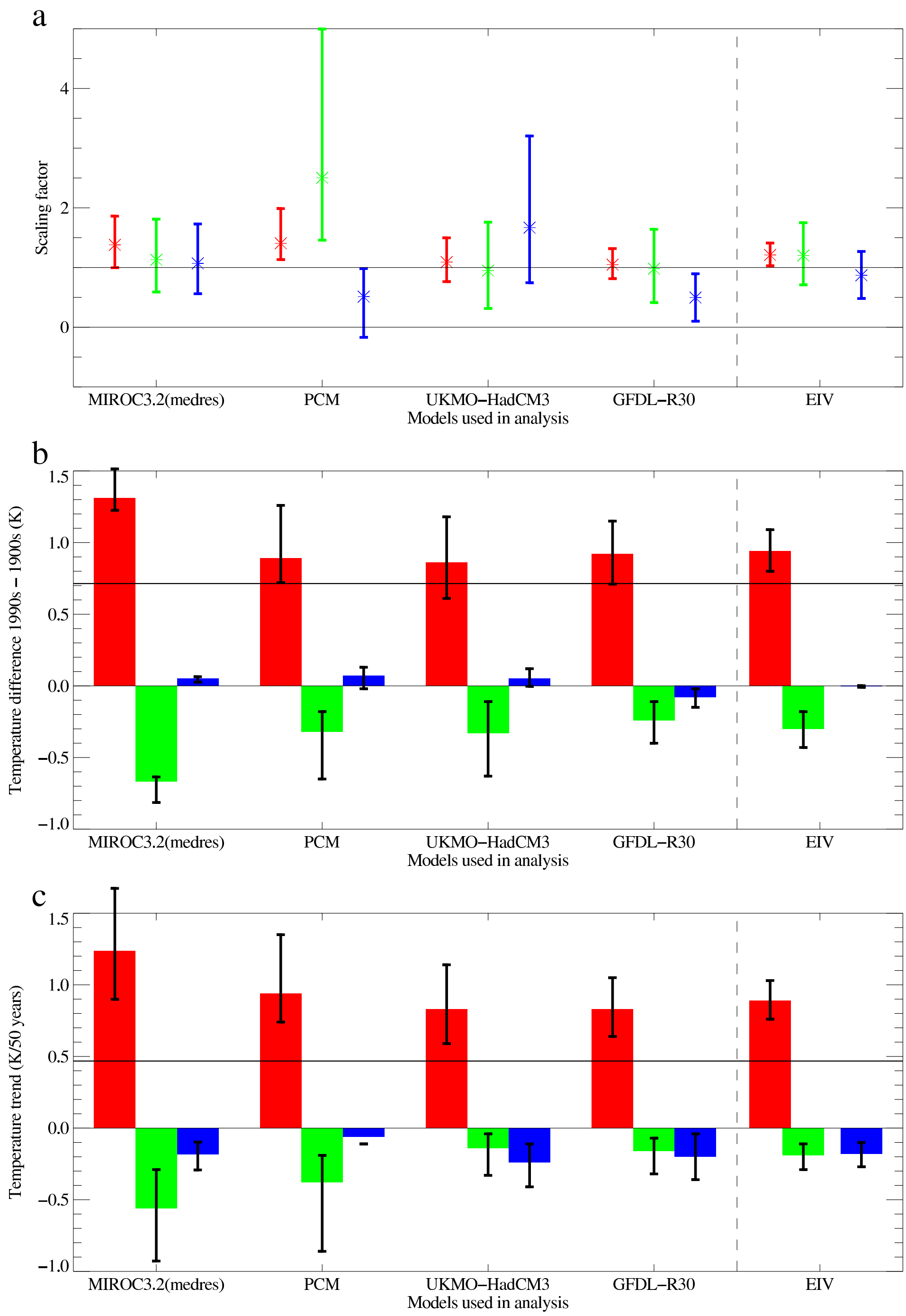

Figure 9.9. Estimated contribution from greenhouse gas (red), other anthropogenic (green), and natural (blue) components to observed global mean surface temperature changes, based on "optimal" detection analyses (Appendix 9.A). Panel a) shows 5 to 95 percentile uncertainty limits on scaling factors (dimensionless), b) the estimated contribution of forced changes to temperature changes over the 20th century, expressed as difference between 1990–1999 mean temperature and 1900–1909 mean temperature (units ºC), and c) estimated contribution to temperature trends over 1950–1999 (units ºC/50-yr). The horizonal black lines in (b) and (c) show the observed temperature changes from HadCRUT2v (Parker et al., 2004). The results of full space-time optimal detection analyses (Nozawa et al., 2005; Stott et al., 2006c) using a total least squares algorithm (Allen and Stott, 2003) from ensembles of simulations containing each set of forcings separately are shown for four models, MIROC3.2(medres), PCM, UKMO-HadCM3 and GFDL-R30. Also shown, labelledby EIV, is an optimal detection analysis using the combined spatio-temporal patterns of response from three models (PCM, UKMO-HadCM3 and GFDL-R30) for each of the three forcings separately and, thus incorporating inter-model uncertainty (Huntingford et al., 2006).

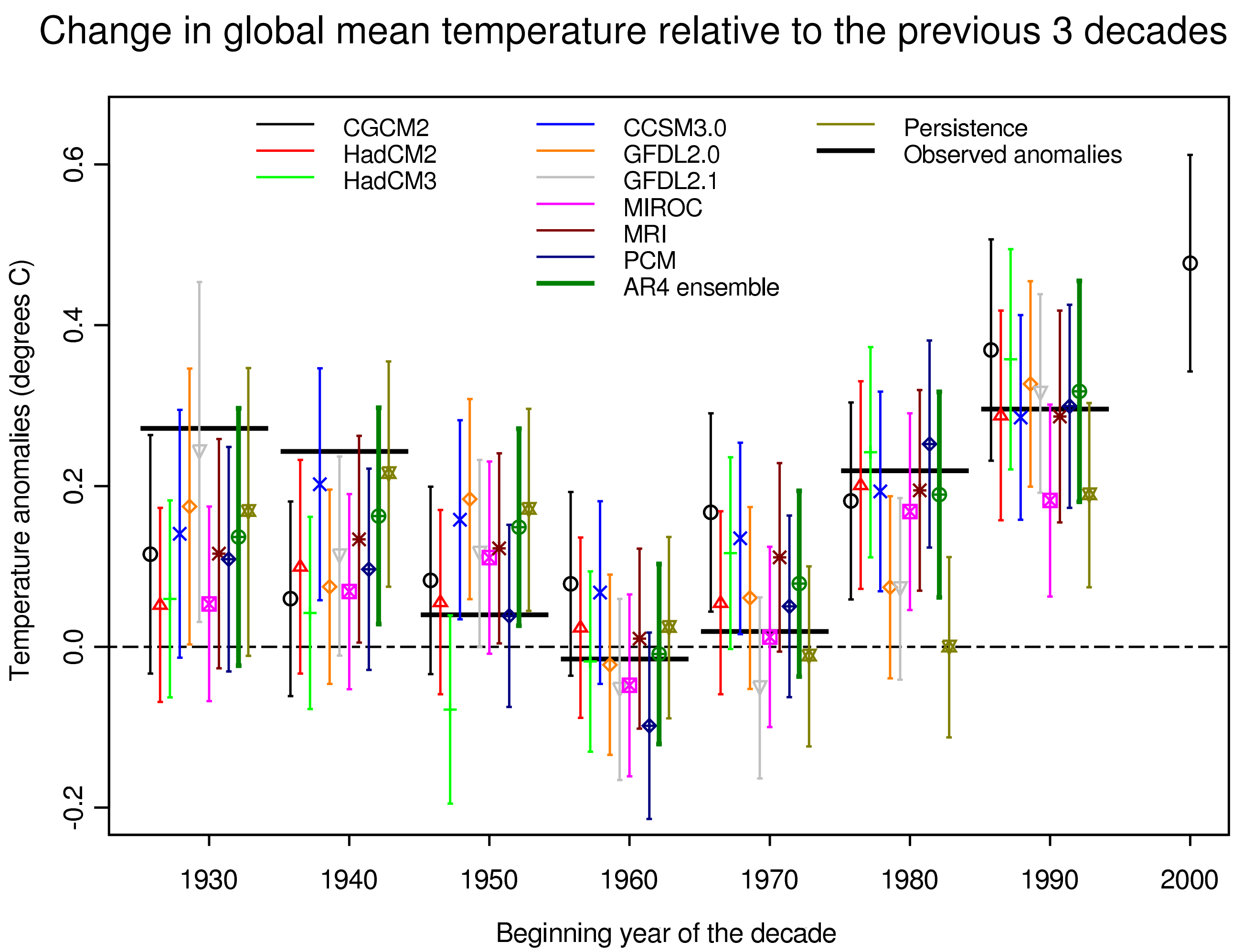

Figure 9.10. Hindcasts and a forecast of global decadal mean surface temperature change based on anthropogenic forcing and their 5–95% confidence bounds. Global decadal mean surface temperature anomalies relative to the preceding 30-year climatology made with CGCM2, HadCM2 (see Chapter 8, Table 8.1, IPCC, 2001) and HadCM3 (model ID 22, Chapter 8, Table 8.1) simulations of the 20th century using anthropogenic forcing only (left hand column of legend) and with simulations from several models in the MMD 20C3M ensemble that use anthropogenic and natural forcings (center column of legend; model IDs 3, 11, 12, 19, 20, 21, Chapter 8, Table 8.1). Hindcasts based on the ensemble mean of the selected 20C3M models are indicated by the thick green line. Observed decadal anomalies relative to the previous three decades are indicated by horizontal black bars. A hindcast based on persisted anomalies from the previous decade is also shown. The hindcasts agree well with observations from the 1950's onwards. Hindcasts for the decades of the 1930's and 1940's are sensitive to the details of the hindcast procedure. A forecast for the decadal global mean anomaly for the decade 2000–2009, relative to the 1970–1999 climatology, based on simulations performed with the CCCma CGCM2 model is also displayed. Units are °C. From Lee et al. (2006).

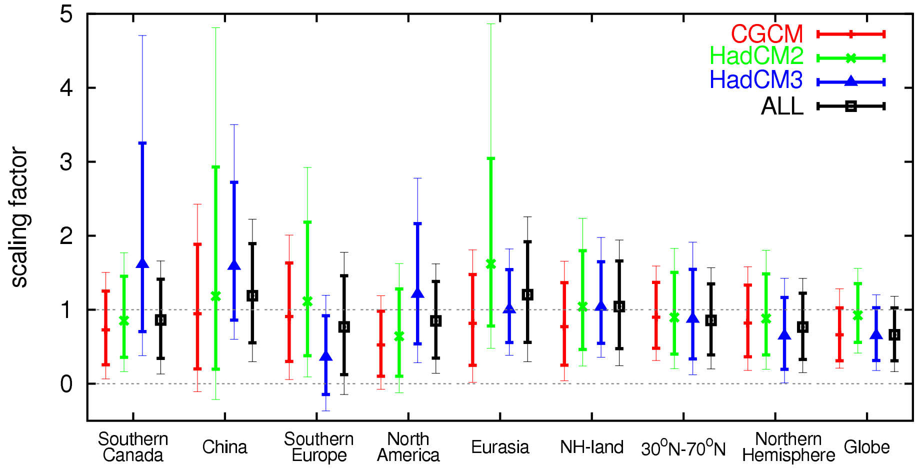

Figure 9.11. Scaling factors indicating the match between observed and simulated decadal near surface air temperature change (1950–1999) when greenhouse gas and aerosol forcing responses (GS) are taken into account in "optimal" detection analyses (Appendix 9.A) on a range of spatial scales from global to sub-continental. Thick bars indicate 90% confidence intervals on the scaling factors, and the thin extensions indicate the increased width of these confidence intervals when estimates of the variance due to internal variability are doubled. Scaling factors and uncertainties are provided for different spatial domains including: Canada (Canadian land area south of 70ºN), China, Southern Europe (European land area bounded by 10ºW–40ºE, 35º–50ºN), North America (North American land area between 30ºN–70ºN), Eurasia (Eurasian land area between 30ºN–70ºN), mid-latitude land area between 30ºN–70ºN (labelled NH-land), the Northern Hemisphere mid-latitudes (30ºN–70ºN including land and ocean), the Northern Hemisphere, and the Globe. The GS signals are obtained from CGCM1 and CGCM2 combined (labeled CGCM, see Chapter 8, Table 8.1, IPCC, 2001), HadCM2 (see Chapter 8, Table 8.1, IPCC, 2001), and HadCM3 (model ID 22, Chapter 8, Table 8.1), and these 4 models combined (labeled ALL). After Zhang et al. (2006); Hegerl et al. (2006c).

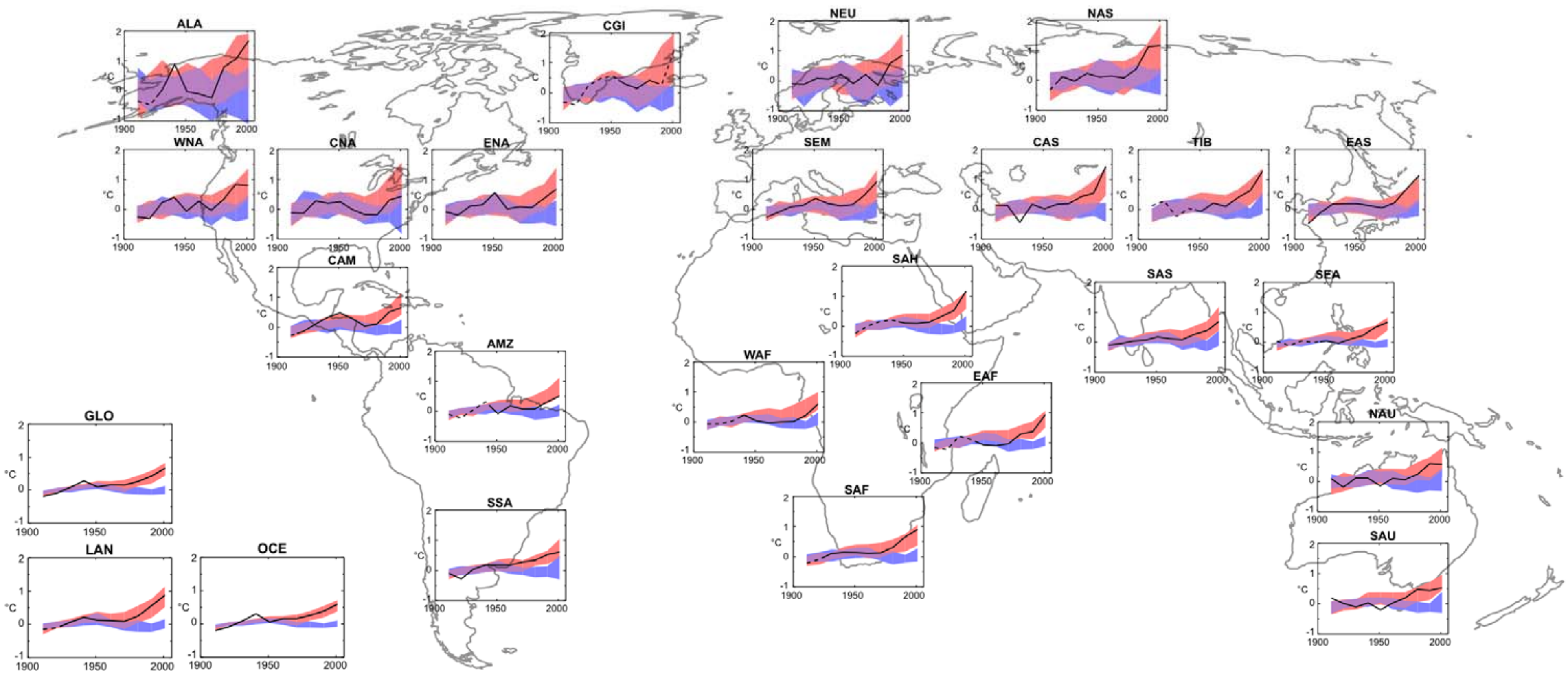

Figure 9.12. Comparison of multi-model dataset 20C3M model simulations containing all forcings (red shaded regions) and containing natural forcings only (blue shaded regions) with observed decadal mean temperature changes 1906-2005 from HadCRUT3 (Brohan et al., 2006). The panel labelled GLO shows comparison for global mean; LAN, global land; and OCE, global ocean data. Remaining panels display results for 22 sub-continental scale regions (see Appendix 9.C for a description of the regions). This figure is produced identically to FAQ 9.2, Figure 1 except the sub-continental regions were used; a full description of the procedures for producing FAQ 9.2, Figure 1 is given in Appendix 9.C. Shaded bands represent the the middle 90% range estimated from the multi-model ensemble. Note that the model simulations have not been scaled in any way. The same simulations are used as in Figure 9.5 (58 all forcings simulations from 14 models, and 19 natural forcings only simulations from 5 models). Each simulation was sampled so that coverage corresponds to that of the observations, and was centred relative to the 1901-1950 mean obtained by that simulation in the region of interest. Observations in each region were centred relative to the same period. The observations in each region are generally consistent with model simulations that include anthropogenic and natural forcings, whereas in many regions the observations are inconsistent with model simulations that include natural forcings only. Units: ºC.

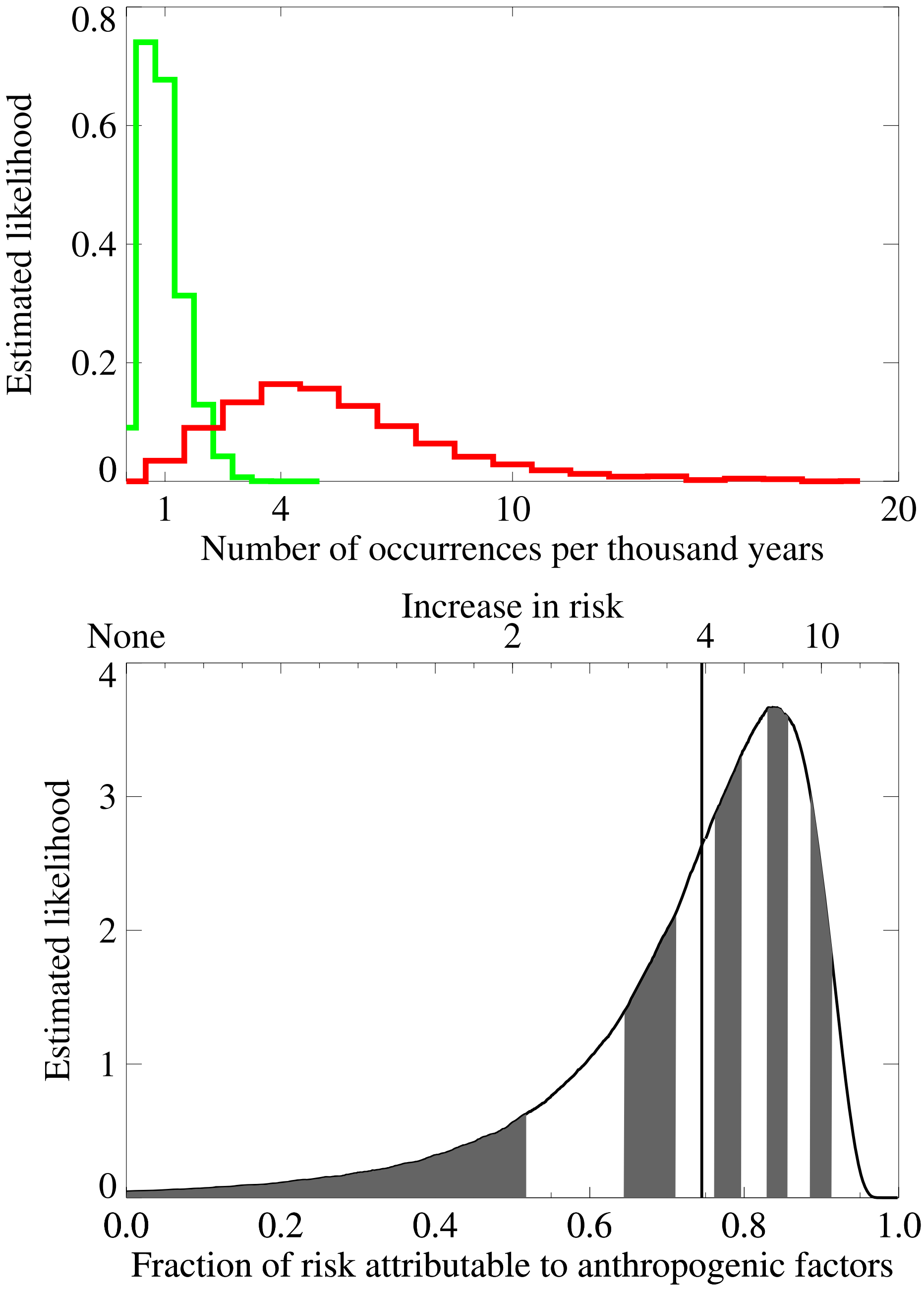

Figure 9.13. Change in risk of mean European summer temperatures exceeding a threshold of 1.6ºC above 1961–1990 mean temperatures, a threshold that was exceeded in 2003 but in no other year since the start of the instrumental record in 1851. a) Frequency histograms of the estimated likelihood of the risk (probability) of exceeding a 1.6°C threshold (relative to the 1961–1990 mean) in the 1990s in the presence (red curve) and absence (green curve) of anthropogenic change, expressed as an occurrence rate. b) Fraction of attributable risk (FAR). Also shown, as the vertical line, is the "best estimate" FAR, the mean risk attributable to anthropogenic factors averaged over the distribution. The alternation between grey and white bands indicates the deciles of the estimated FAR distribution. The shift from the green to the red distribution (a) implies a FAR distribution whose mean is 0.75, corresponding to a four-fold increase in the risk of such an event (b). From Stott et al. (2004).

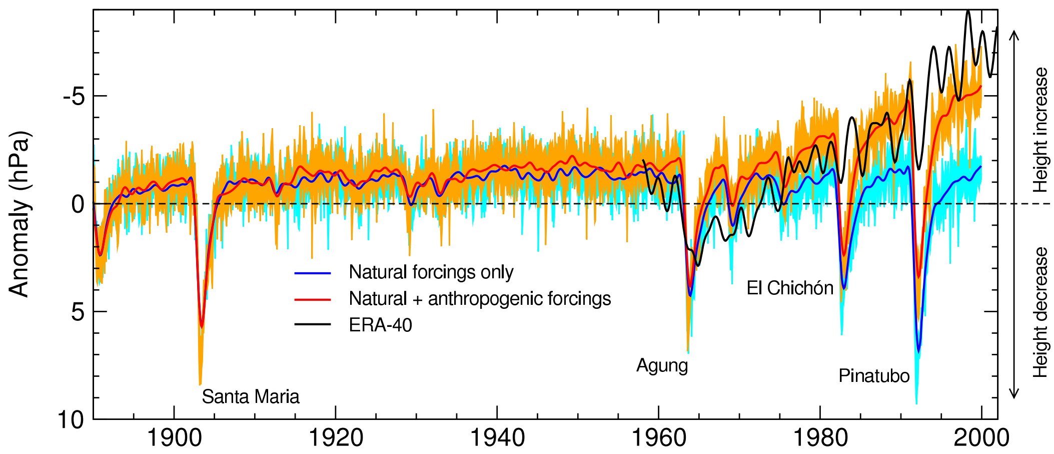

Figure 9.14. Comparison between reanalysis and climate-model simulated global monthly mean anomalies in tropopause height. Model results are from two different PCM (model ID 21, Chapter 8, Table 8.1) ensemble experiments using either natural forcings (SV), or natural and anthropogenic forcings (ALL). There are four realizations of each experiment. Both the low-pass filtered ensemble mean and the (unfiltered) range between the highest and lowest values of the realizations are shown . All model anomalies are defined relative to climatological monthly means computed over 1890–1999. Reanalysis based tropopause height anomalies estimated from ERA-40 were filtered in the same way as model data. The ERA-40 record spans 1957–2002 and was forced to have the same mean as ALL over 1960–1999 (1979–1993). From Santer et al. (2003a).

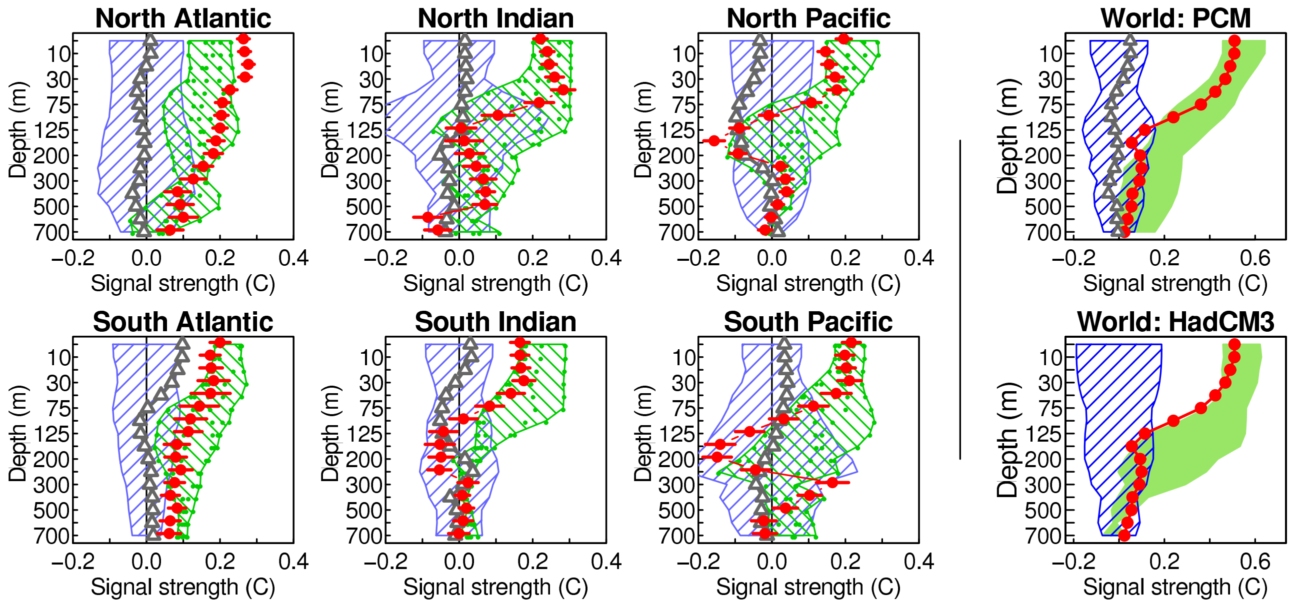

Figure 9.15. Strength of observed and model-simulated warming signal by depth for the world ocean and for each ocean basin individually. For ocean basins the signal is estimated from PCM (model ID 21, Chapter 8, Table 8.1) while for the world ocean it is estimated from both PCM and HadCM3 (model ID 22, Chapter 8, Table 8.1). Red dots represent the projection of the observed temperature changes onto the normalised model-based pattern of warming. They show substantial basin-to-basin differences in how the oceans have warmed over the past 40 years, although all oceans have experienced net warming over that interval. The red bars represent the ± two standard deviation limits associated with sampling uncertainty. The blue cross hatched swaths represent the 90% confidence limits of the natural internal variability strength. The green cross hatched swaths represent the range of the anthropogenically forced signal estimates from different realizations of identically forced simulations with the PCM model for each ocean basin (the smaller dots within the green swaths are the individual realizations) and the green shaded regions represent the range of anthropogenically forced signal estimates from different realizations of identically forced simulations with the PCM and HadCM3 models for the world ocean (note that PCM and HadCM3 use different represenations of anthropogenic forcing). The ensemble averaged strength of the warming signal in four PCM simulations with solar and volcanic forcing is also shown (grey triangles). From Barnett et al. (2005) and Pierce et al. (2006).

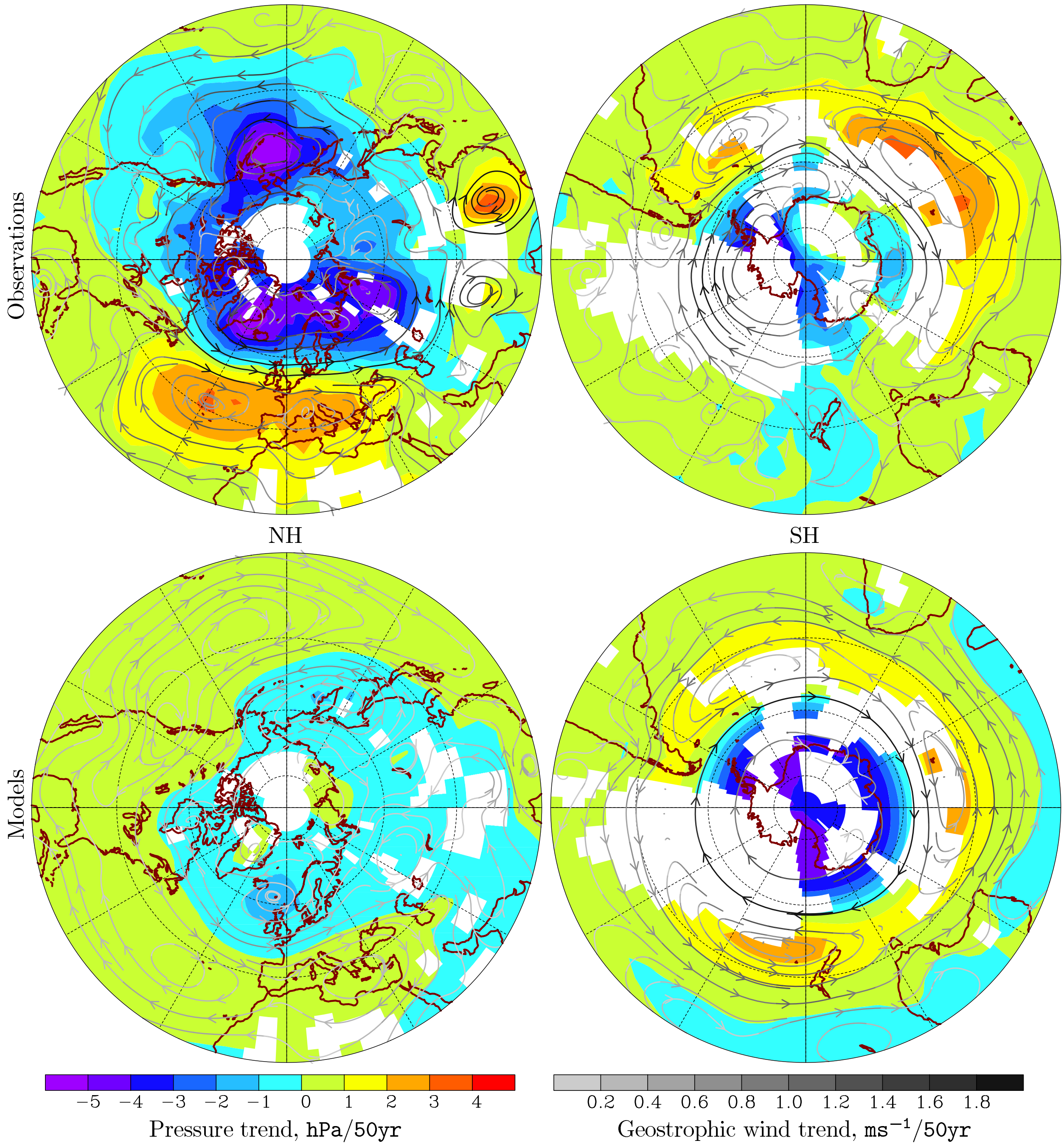

Figure 9.16. Comparison between observed (top) and model-simulated (bottom) December-February sea-level pressure trends based on decadal means for the period 1955–2005. Observed trends are based on HadSLP2r (an infilled observational dataset, Allan and Ansell, 2006), and the mean simulated response to greenhouse gas, sulphate aerosol, stratospheric ozone, volcanic aerosol, and solar irradiance changes in eight IPCC AR4 coupled models (CCSM3, GFDL-CM2.0, GFDL-CM2.1, GISS-EH, GISS-ER, MIROC3.2(medres), PCM, UKMO-HadCM3; model IDs 3, 11, 12, 14, 15, 19, 21 and 22, Chapter 8, Table 8.1) . Streamlines indicate the direction of the trends in the geostrophic wind derived from the trends in sea-level pressure, and the shading of the streamlines indicates the magnitude of the change, with darker streamlines corresponding to larger changes in geostrophic wind. Both observations and model data are blanked out where there are insufficient station-based measurements to constrain analysis. Further explanation of the construction of this figure is provided in Appendix 9.C. Units: hPa/ 50 yr (SLP), m/s/ 50 yr (wind velocity). Updated after Gillett et al. (2005).

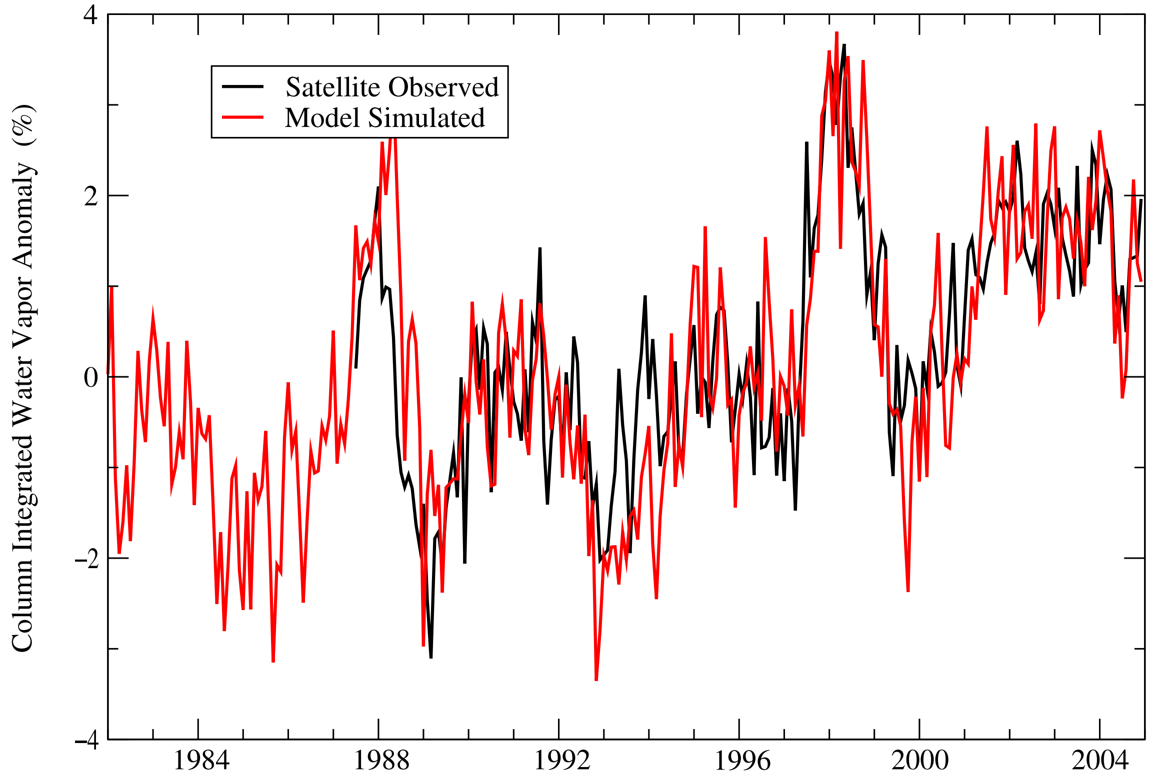

Figure 9.17. Global mean (ocean-only) anomalies in column integrated water vapour from simulations with the Geophysical Fluid Dynamics Laboratory (GFDL) AM2-LM2 atmospheric GCM forced with observed sea surface temperatures (red), and satellite observations from SSMI (black, Wentz and Schabel, 2000)). From Soden et al. (2005).

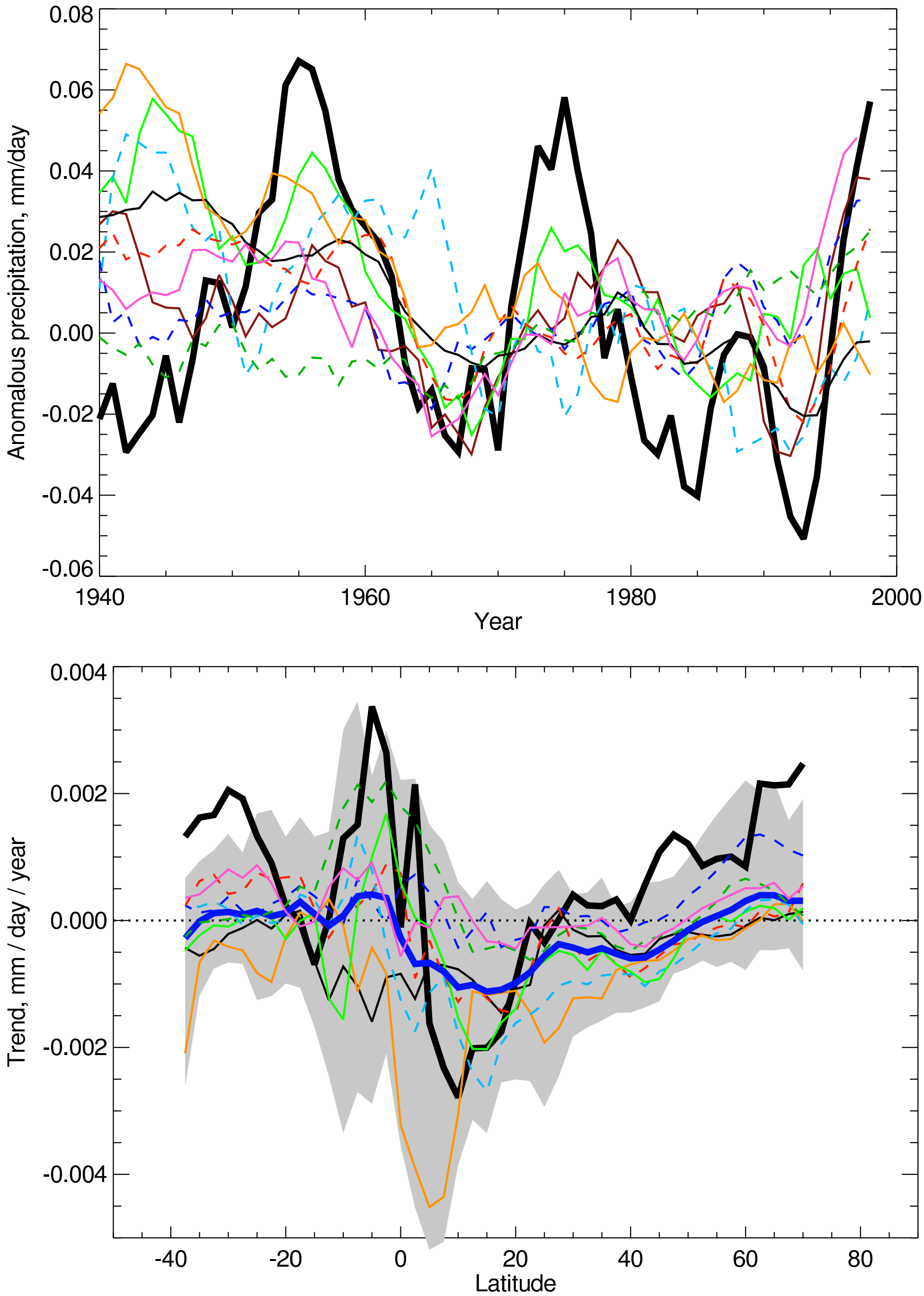

Figure 9.18. Simulated and observed anomalies in terrestrial mean precipitation (a), and zonal mean precipitation trends (b). Observations are based on a gridded data set of terrestrial rain gauge measurements (New et al., 2000) (thick black line). Model data are from 20th century multi-model dataset integrations with anthropogenic, solar, and volcanic forcing from the following coupled climate models: UKMO-HadCM3 (model ID 22, Chapter 8, Table 8.1, brown), CCSM3 (3, dark blue), GFDL-CM2.0 (11, pale green), GFDL-CM2.1 (12, pale blue), GISS-EH (14, red), GISS-ER (15, thin black), MIROC3.2(medres) (19, orange), MRI-CGCM2.3.2 (20, dark green), and PCM (21, pink). Coloured curves are ensemble means from individual models. In (a), a five year running mean was applied to suppress other sources of natural variability, such as ENSO. In (b), the grey band indicates the range of trends simulated in individual ensemble members, and the thick dark blue line indicates the multi-model ensemble mean. External influence in observations of global terrestrial mean precipitation is detected with those precipitation simulations shown by continuous lines in the top panel. Adapted from Lambert et al. (2005).

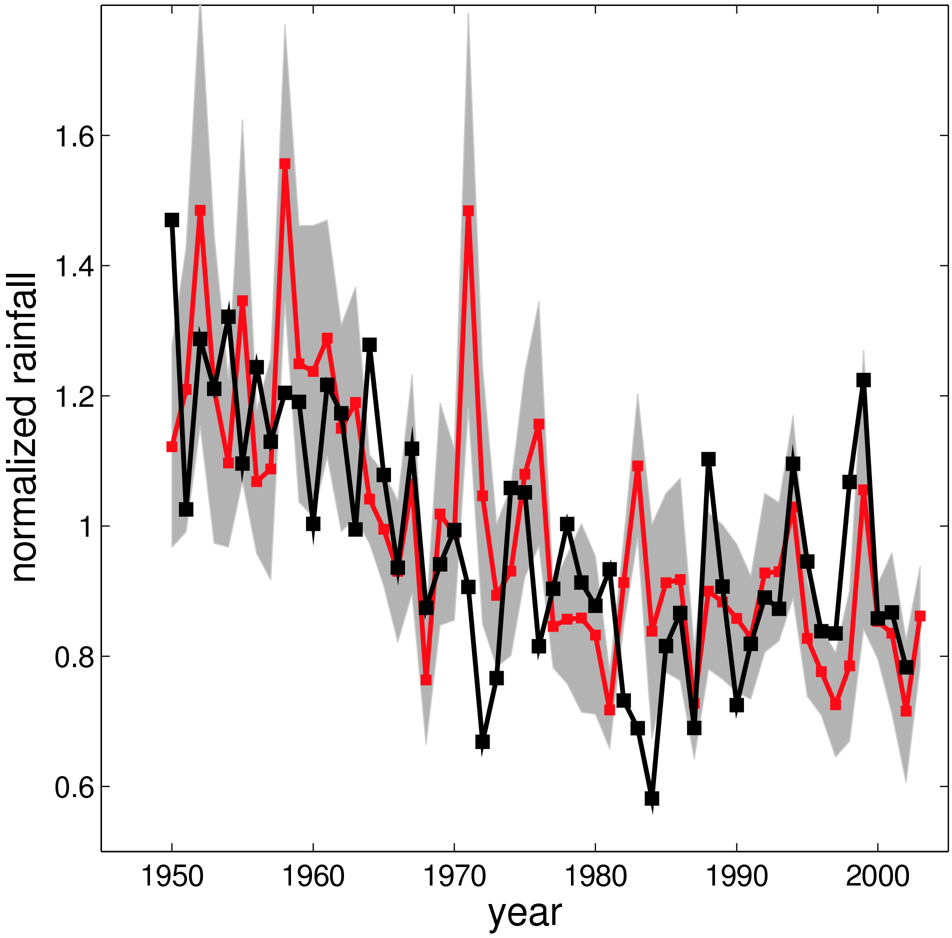

Figure 9.19. Observed (CRU-TS2.1, Mitchell and Jones, 2005) Sahel July-September rainfall for each year (black), compared to an ensemble mean of 10 simulations of the atmospheric/land component of GFDL-CM2.0 model forced with observed sea surface temperatures (red). The grey band represents ± one standard deviation of intra-ensemble variability. From Held et al. (2005), based on results in Lu and Delworth (2005).

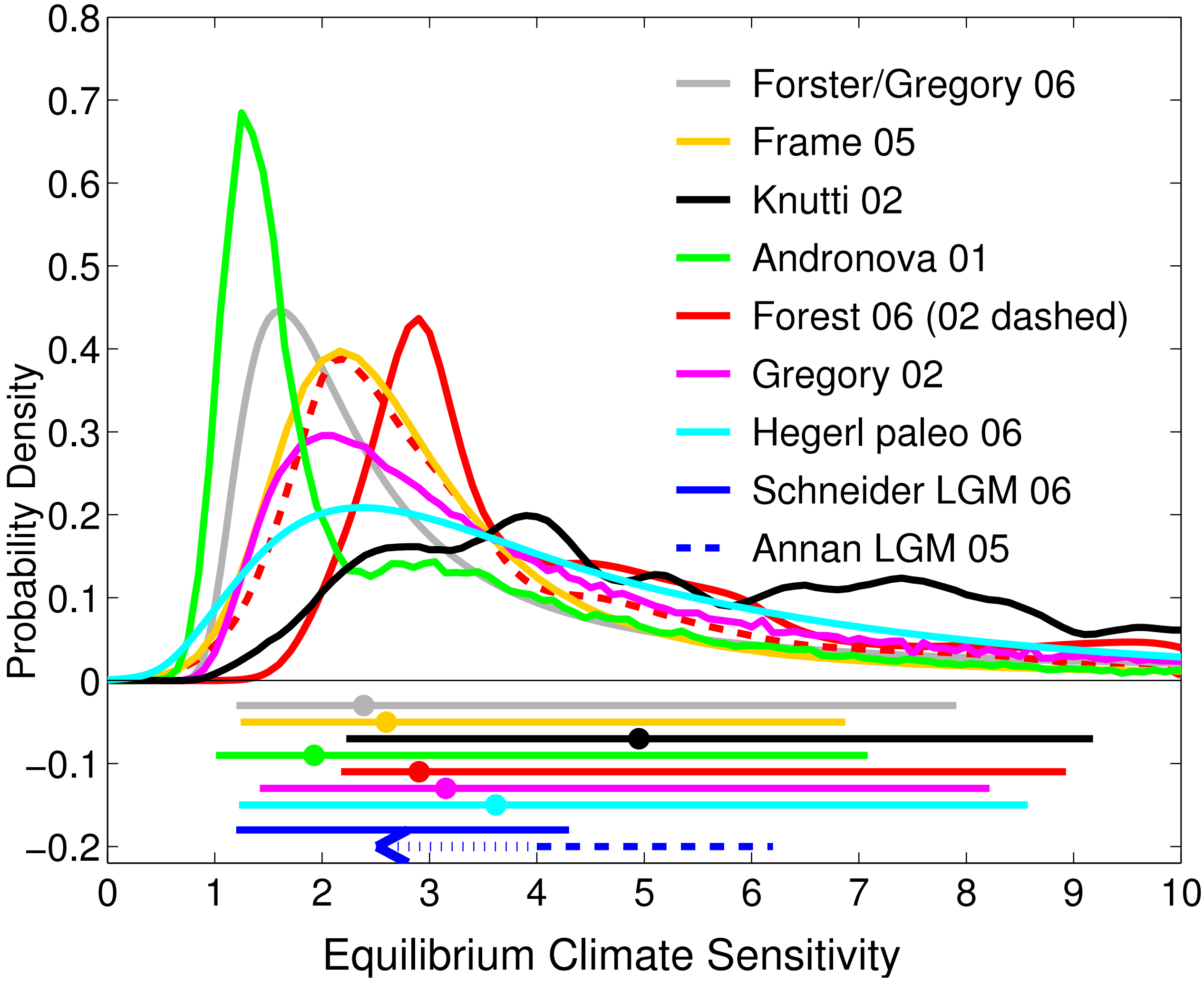

Figure 9.20. Comparison between different estimates of the probability density function (or relative likelihood) for equilibrium climate sensitivity. All PDFs/likelihoods have been scaled to integrate to 1 between 0 and 10. The bars show the respective 5–95% ranges, dots the median estimate. Pdfs/likelihoods based on instrumental data are from Andronova and Schlesinger (2001), Forest et al. (2002) (dashed line, considering anthropogenic forcings only), Forest et al. (2006) (solid, anthropogenic and natural forcings), Gregory et al. (2002a), Knutti et al. (2002), Frame et al. (2005), and Forster and Gregory (2006), transformed to a uniform prior in ECS using the method after Frame et al. (2005). Hegerl et al. (2006a) is based on multiple paleo reconstructions of Northern Hemispheric mean temperatures of the last 700 years. Also shown are the 5–95% approximate ranges for two estimates from the Last Glacial Maximum (dashed, Annan et al., 2005; solid, Schneider von Deimling et al., 2006) which are based on models with different structural properties. Note that ranges extending beyond published range in Annan et al. (2005), and beyond that sampled by the climate model used there, are indicated by dots and an arrow, since Annan et al. only provide an upper limit. For details in likelihood estimates see Table 9.3. After Hegerl et al. (2006a)

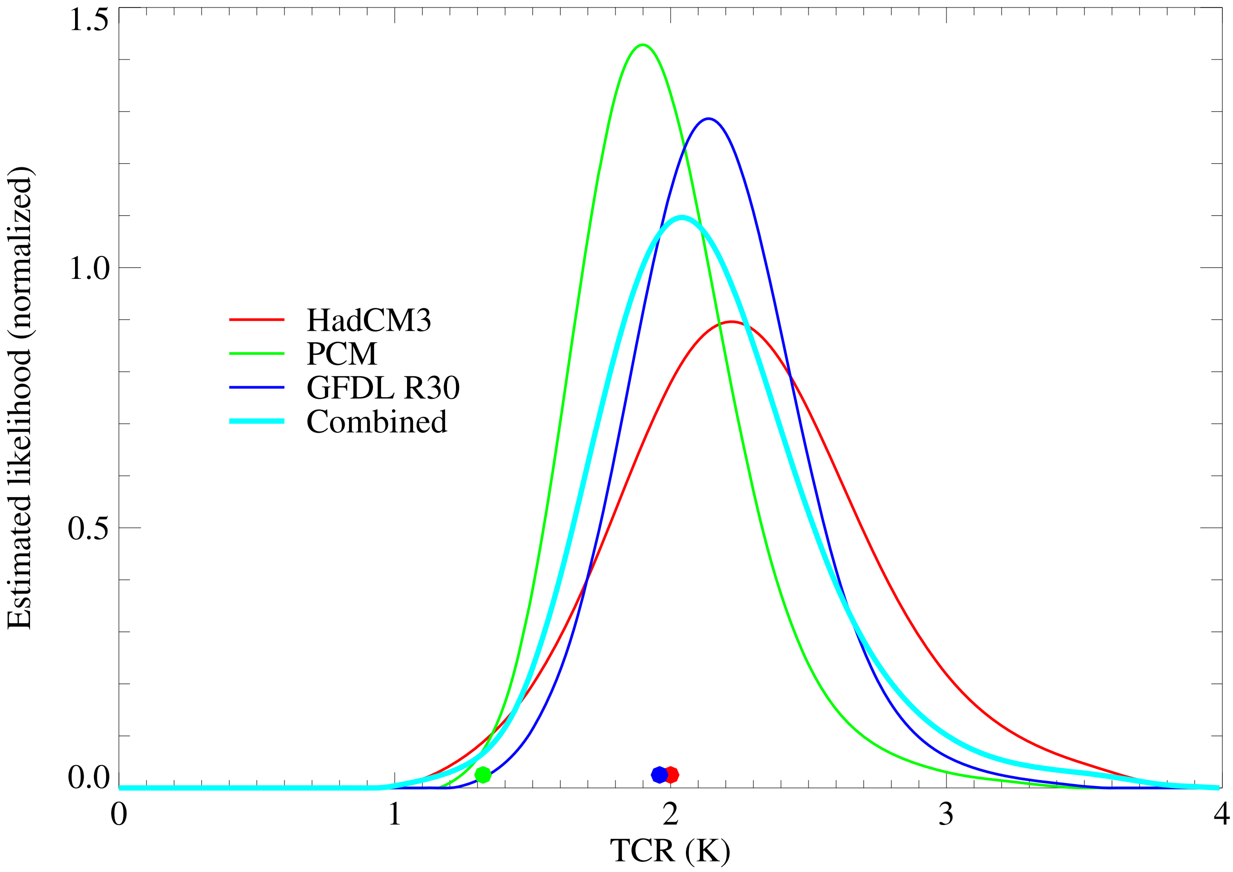

Figure 9.21. Probability distributions of transient climate response (TCR, expressed as warming at the time of CO2 doubling), as constrained by observed 20th century temperature change, for HadCM3 (model ID 22, Chapter 8, Table 8.1, red), PCM (21, green), GFDL R30 (Delworth et al., 2002, blue) models and averaging the PDFs derived from each model (turquoise). Coloured stars show each model's TCR. (From Stott et al., 2006c).

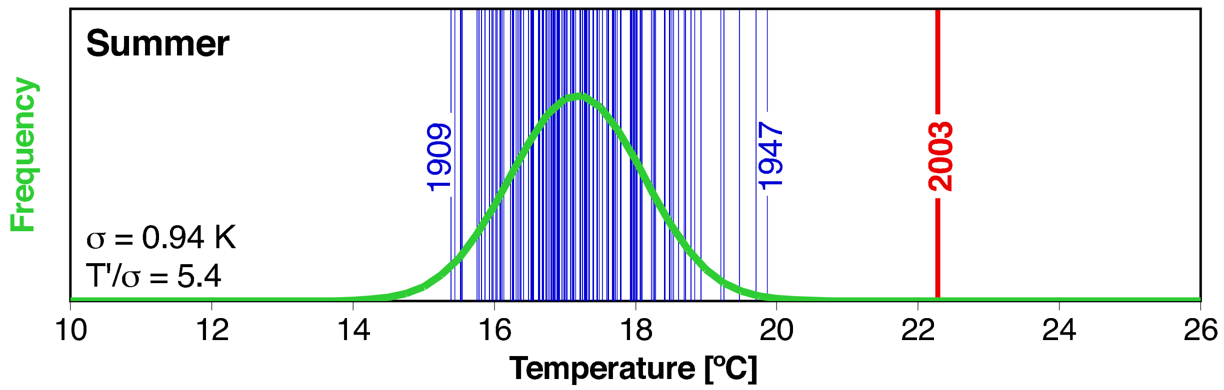

FAQ 9.1, Figure 1. Summer temperatures in Switzerland from 1864 to 2003 are, on average, about 17°C, as shown by the green curve. During the extremely hot summer of 2003, average temperatures exceeded 22° C., as indicated by the red bar. (A vertical line is shown for each year in the 137-yr record. The fitted Gaussian distribution is indicated in green. The years 1909, 1947, and 2003 are labeled because they represent extreme years in the record. The values in the lower left corner indicate the standard deviation (σ) and the 2003 anomaly normalized by the 1864–2000 standard deviation (T'/ σ)). From Schär et al. (2004).

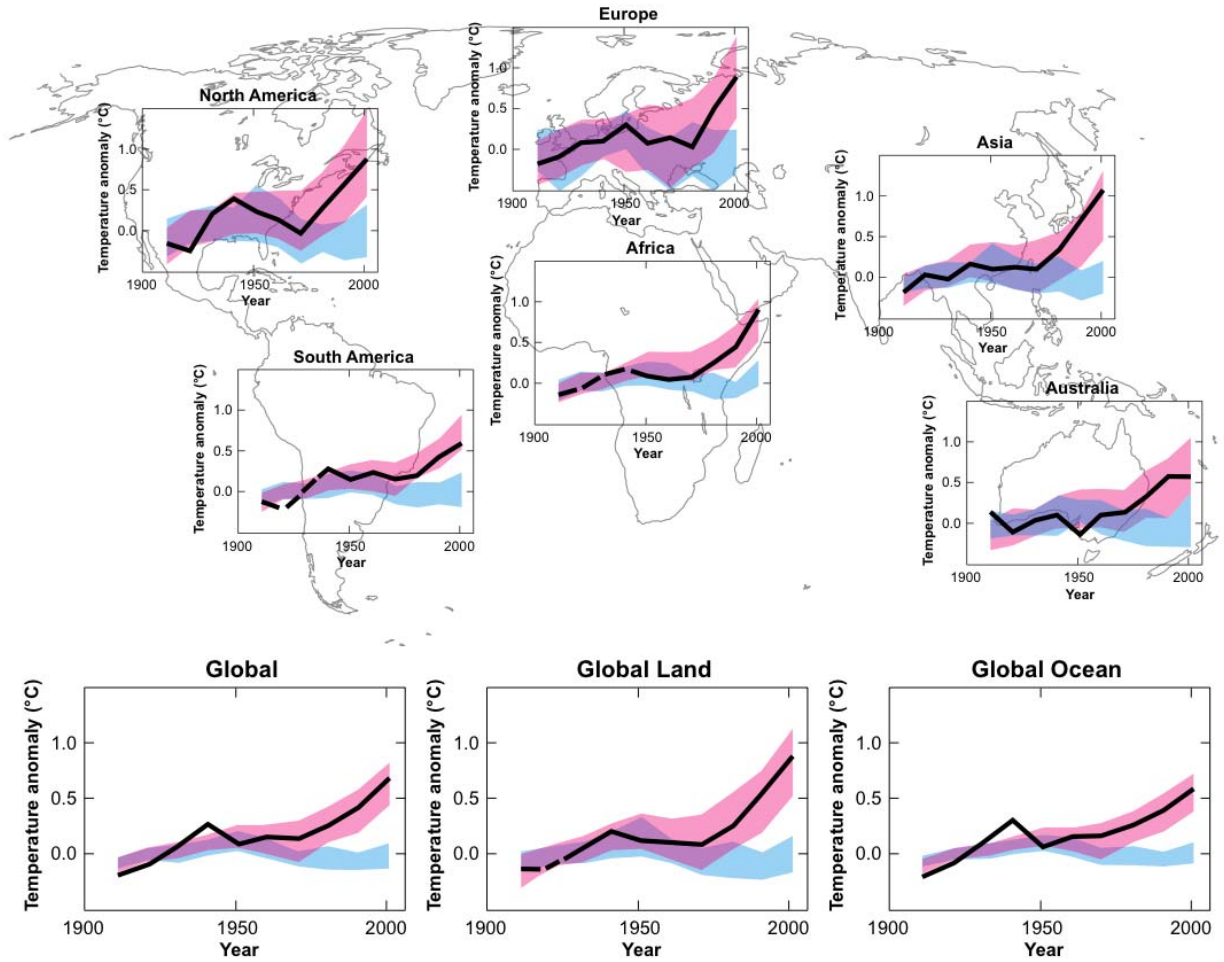

FAQ 9.2, Figure 1. Temperature changes in °C from decade to decade during the last century over the Earth's continents, as well as the entire globe, global land area, and the global ocean (lower graphs). The black line indicates observed temperature change, while the coloured bands show the combined range covered by 90% of recent model simulations -- red indicates simulations which include natural and human factors, while blue indicates simulations which include only natural factors. Dashed black lines indicate decades and continental regions for which there are substantially fewer observations. Detailed descriptions of this figure and the methodology that was used in its production are given in Appendix 9.C.